

Ultrafast dynamics in atoms, molecules, and clusters induced by an XFEL pulse

In early 2012, an X-ray free-electron laser (XFEL) facility, the SPring-8 Angstrom Compact free electron LAser (SACLA) [1], started user operation in Japan. Intense pulses generated by SACLA, together with advanced imaging and spectroscopic techniques, have opened new avenues to solve new structures and to observe structural changes in any form of matter with an unprecedented combination of spatial and temporal resolutions. One of the promising studies using XFELs may generally be single-shot X-ray imaging based on the “before destroy” concept. However, target samples should be affected by ultrafast reactions occurring during XFEL pulse exposure. To utilize XFEL for “before destroy” imaging, it is indispensable to understand what happens in the matter during XFEL pulse exposure. The ultrafast reaction dynamics in atoms, molecules, and atomic clusters in the gas phase are not only fundamentally interesting but also fundamentally important for this purpose. Thus, we have been investigating the ultrafast reaction dynamics in atoms [2], molecules [3,4], and clusters [5,6,7] irradiated by XFEL pulses. In this article, we review some of our investigations that we carried out at SACLA during its first five years.

Experiment

A series of experiments have been carried out at SACLA BL3 [8]. An XFEL beam was focused by a Kirkpatrick-Baez mirror system to

a focal point of $\sim 1 \mu\text{m}$ (FWHM) diameter. Target samples were introduced into a reaction chamber as a supersonic gas beam. XFEL pulse energies were measured by the beam position monitor located upstream of the beamline. The relative X-ray pulse energy passing through the interaction point was also measured shot-by-shot by a PIN photodiode.

Ions and electrons emitted from the gas-phase samples irradiated by very intense XFEL pulses were detected by the momentum spectrometers developed specifically for such XFEL experiments. Details of our setups are described in [9]. In brief, ions generated in the reaction volume were extracted towards an ion time-of-flight (TOF) spectrometer equipped with microchannel plates (MCPs) and a delay-line anode (RoentDek HEX80). Signals from the delay-line anode and MCPs were recorded by a digitizer and analyzed by a software discriminator. The arrival time and arrival position of each ion were determined. Three-dimensional momenta of individual ions were calculated using the detected position and TOF information of each ion. Electrons generated in the reaction volume were extracted towards a velocity map imaging (VMI) spectrometer equipped with MCPs and a phosphor screen. Electron detection images on the phosphor screen were recorded using a CCD camera synchronized with

the arrival of the XFEL pulse in the interaction chamber. The measured two-dimensional projection allows us to obtain the momentum distributions of the ejected electrons using the inverse Abel transformation.

Multiphoton multiple ionization dynamics in xenon atom

Figure 1 depicts the charge state distribution of Xe ions generated by irradiating Xe atoms with an XFEL pulse at a photon energy of 5.5 keV and a peak fluence of $47 \mu\text{J}/\mu\text{m}^2$ [2]. We compared the theoretical charge state distributions at this peak fluence with the experimental distributions. The photon energy of 5.5 keV is above the L-shell threshold for charge states of up to +23 according to the calculations [2]. Thus, direct two-photon ionization barely contributes to charge formation because not only is its cross section very small but also one-photon ionization is always available up to +23. There is no apparent signature of resonance-enabled ionization enhancement because the fluence is insufficient to

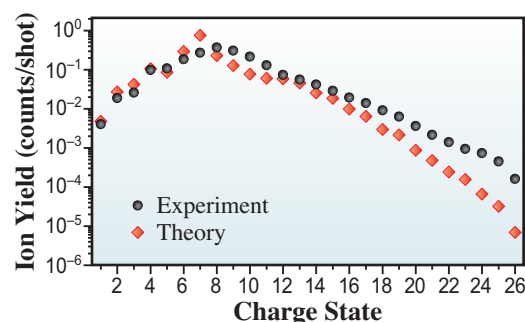


Fig. 1. Experimental and theoretical charge state distributions of Xe at a photon energy of 5.5 keV. The peak fluence is $47 \mu\text{J}/\mu\text{m}^2$. [2]

form high charge states that involve resonance excitation. The discrepancy between theory and experiment may be attributed to the nonrelativistic treatment and lack of shake-off in the current theoretical model. The shake-off process can further ionize valence electrons after photoionization, and some decay channels might be absent without relativity. The inclusion of both relativity and shake-off tends to produce higher charge states. In spite of these limitations, the theoretical results are in reasonable agreement with experimental results, at least semiquantitatively.

The charge state distribution varies with the peak fluence. The peak fluence dependence of the ion yield for each charge state indicates contributions from multiphoton processes. According to the peak fluence dependence and theoretical calculations, the observed high charge states with ≥ 24 are produced via five-photon absorption. Understanding of the ionization dynamics of heavy atoms exposed to intense XFEL pulses will provide us with useful input for future molecular imaging experiments using XFELs.

Charge and nuclear dynamics in iodine-containing molecules

In the case of the irradiation of molecules by XFEL pulses, in addition to multiphoton absorption and charge buildup we observed in atoms, charge redistribution and bond rupture occur, resulting in the generation of several ions from a single molecule. Ions released from a single molecule must have a momentum correlation. As the first molecular sample, we used the iodomethane (CH_3I) molecule, which is the smallest organic molecule that contains a heavy iodine atom. Figure 2 depicts an example of correlations between the momenta of C^{n+} and I^{m+} released from CH_3I irradiated by an XFEL pulse [3]. The photon energy was 5.5 keV and the peak fluence was $26 \mu\text{J}/\mu\text{m}^2$. Here, the momentum

correlation coefficient k_{mn} is the average ratio of the momenta of C^{n+} and I^{m+} . The experimental results are well reproduced by a simple Coulomb explosion model with a few physically meaningful empirical constants that account for the concerted dynamics of nuclear motion vs charge creation and redistribution. According to the results of model calculations, we found that it takes ~ 9 fs for the charge to be created at the iodine site, while it takes ~ 3 fs for the charge to be redistributed among the molecules. Also, we found that the C–I bond length increases by $\sim 10\%$, whereas the C–H bond distance increases by a factor of three in 10 fs. In this way, the electron and nuclear motions during XFEL pulse exposure can be captured.

As the next target sample, we adopted a larger molecule, 5-iodouracil ($\text{C}_4\text{N}_2\text{O}_2\text{H}_3\text{I}$, 5IU) [4]. 5IU is an iodine-substituted molecule of uracil, which is one of the RNA bases. Thus, 5IU is considered to be the smallest building block of biomolecules. Figure 3 depicts momentum correlations among three ions released from 5IU. To observe the correlations, a triple product was calculated from the observed momenta, giving the cosine of the polar angle:

$$\cos(\varphi) = \frac{(\mathbf{p}_A \times \mathbf{p}_B) \cdot \mathbf{p}_C}{|\mathbf{p}_A \times \mathbf{p}_B| |\mathbf{p}_C|},$$

where \mathbf{p}_A , \mathbf{p}_B , and \mathbf{p}_C are the momentum vectors of ions A, B, and

C, respectively. The experimental distributions, denoted as $\text{SP}_3(\text{A,B,C})$, are depicted in the left column of Fig. 3. Note that the distribution function SP_3 for three randomly oriented and uncorrelated vectors is flat against $\cos(\varphi)$ and thus the curves presented directly reflect the deviation from isotropic emission. Coulomb explosion, when it occurs preferentially in the plane, results in the distributions of $\text{SP}_3(\text{A,B,C})$ peaked at $\cos(\varphi)=0$. As seen in the figure, the combinations $\text{SP}_3(\text{I}^{q+}, \text{H}^+, \text{X})$, where X stands for H^+ , O^+ , N^+ , or C^+ . I^{q+} , H^+ , N^+ , and O^+ , tend to be ejected preferentially in the plane, but this is not necessarily the case for C^+ . The discrepancies between the experimental and simulated $\text{SP}_3(\text{I}^{q+}, \text{H}^+, \text{C}^+)$ for high q are probably due to the existence of molecular and neutral fragments, which are not considered in the simulation.

To interpret the experimental results and quantify the underlying dynamics, we carried out classical molecular dynamics (MD) simulations of Coulomb explosion within a parametric model of charge buildup and redistribution. Good agreement between the experimental and simulation results was found when selecting the internal temperature, charge buildup time, and charge redistribution rate of 300 K, 10 fs, and 0.5 fs^{-1} , respectively. The simulation results are shown in the right column of Fig. 3. The time dependence of

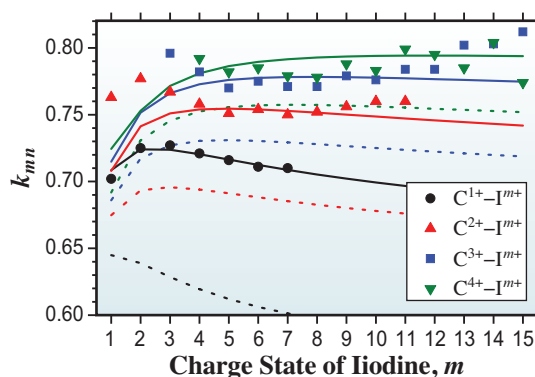


Fig. 2. Momentum correlation coefficient k_{mn} for I^{m+} – C^{n+} coincidences at a photon energy of 5.5 keV. The peak fluence is $26 \mu\text{J}/\mu\text{m}^2$. [3]

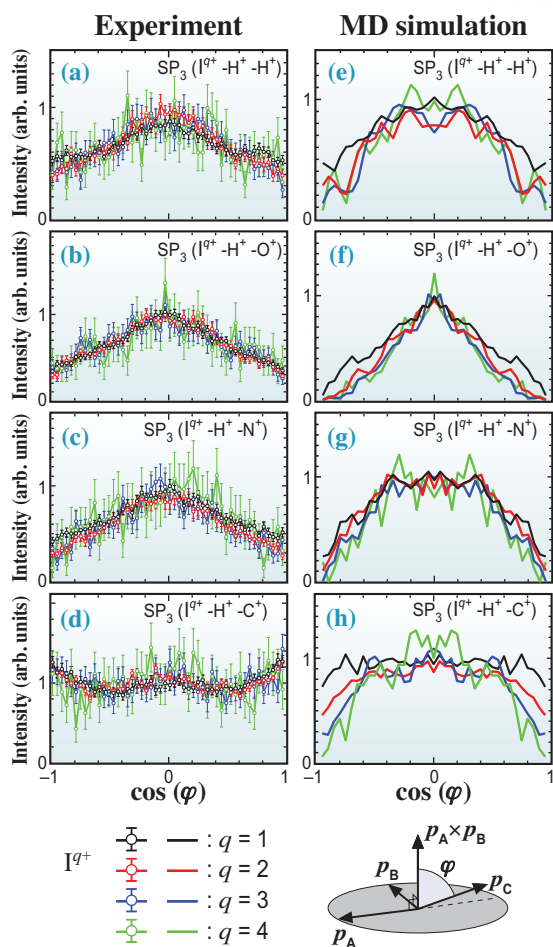


Fig. 3. Distributions of normalized scalar triplet products of momentum vectors $SP_3(A,B,C)$ plotted as a function of $\cos(\varphi)$. Black, red, blue, and green lines indicate $q = 1, 2, 3,$ and 4 , respectively. [4]

the interatomic distances, deduced from the MD simulations, suggests that within 10 fs, the displacements are large for hydrogens and are considerably smaller, within 10% of the bond length variation, for other heavier atoms.

Nanoplasma dynamics in atomic clusters

It is known that nanoplasma is formed when clusters (i.e., atomic or molecular aggregates) are irradiated by intense lasers with longer wavelengths, e.g., near infrared (NIR) lasers. What will happen to clusters exposed to intense XFEL pulses? Figure 4 depicts the electron spectra of

Ar clusters with different average cluster sizes $\langle N \rangle$ exposed to an XFEL pulse at a photon energy of 5 keV [5]. The peak fluence of the XFEL pulses was $\sim 50 \mu\text{J}/\mu\text{m}^2$. In the spectrum for $\langle N \rangle \sim 100$, we can identify the broad peak around 150–250 eV due to the LMM Auger electrons emitted after the KLL Auger process. The intensity of electron emission below 150 eV increases with the cluster size. This trend is interpreted in the following manner, with the help of theoretical calculations that reproduce the experimental spectra as shown in Fig. 4. The discrepancies between the experimental and theoretical spectra, caused by the uncertainties of the cluster size and size distributions, do not affect the following discussion. When the cluster is exposed to intense XFEL pulses, atoms in the cluster are ionized by photoionization and subsequently proceeding Auger decays. The charge state of the cluster increases with the number of ionized atoms. As a result, the LMM

Auger electrons are decelerated by the positive potential from the highly charged cluster and form a plateau in the electron spectra. The decelerated electrons are eventually trapped by the cluster ions. The LLM Auger electrons and the secondary electrons produced by the low-energy electron impact are also trapped. As a result, we expect that a nanoplasma is formed. The peak at zero kinetic energy is due to thermal emission, which is evidence of nanoplasma formation. Note that nanoplasma formation can always occur whenever matter is exposed to an intense XFEL pulse.

For further investigation, we employed pump–probe measurements using the XFEL pulse as a pump and the NIR laser pulse as a probe [7]. To observe ultrafast phenomena, we used an arrival timing monitor [10] to compensate for the temporal jitter between the two laser pulses. Time-resolved yields of ions released from Xe clusters ($\langle N \rangle \sim 5000$) were measured. The photon energies of the XFEL and NIR laser pulses were 5.5 keV and 1.5 eV, respectively. The peak fluences of the XFEL and NIR laser pulses were $30 \mu\text{J}/\mu\text{m}^2$ and $15 \text{ nJ}/\mu\text{m}^2$, respectively.

Figure 5 depicts Xe^+ and Xe^{2+} yields as a function of pump–probe delay. Let us first focus on the Xe^{2+} yield [7]. In Fig. 5, a gradual increase in Xe^{2+} yield with the time delay can be observed. The electrons in

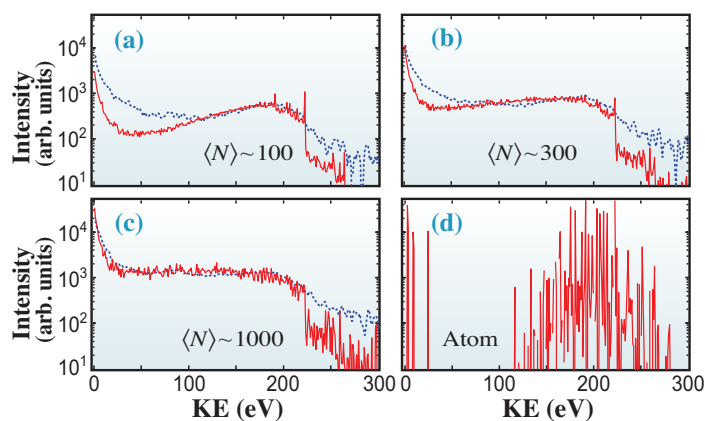


Fig. 4. Electron spectra of Ar clusters at a photon energy of 5 keV. The peak fluence was $\sim 50 \mu\text{J}/\mu\text{m}^2$. Blue dotted lines are the experimental results and red solid lines are the corresponding theoretical results. [5]

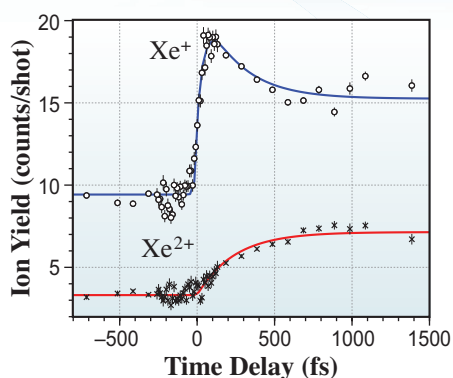


Fig. 5. Xe^+ and Xe^{2+} yields as a function of the time delay of the NIR-probe pulse (1.5 eV) with respect to the XFEL-pump pulse (5.5 keV). The peak fluences of the XFEL and NIR laser pulses were $30 \mu\text{J}/\mu\text{m}^2$ and $15 \text{ nJ}/\mu\text{m}^2$, respectively. [7]

the nanoplasma produced by XFEL irradiation acquire kinetic energy from the additional NIR laser field and further ionize neutral Xe to Xe^+ and Xe^+ to Xe^{2+} by collisional ionization processes. The gradual increase in Xe^{2+} yield indicates the following. Quasi-free electrons in the nanoplasma are so dense that they shield the electric field inside the nanoplasma when the nanoplasma is formed. Then, the electron density decreases with time owing to the nanoplasma expansion. With the decrease in electron density, the nanoplasma starts to absorb NIR light more efficiently via the surface plasmon resonance effect.

In contrast to the gradual increase in Xe^{2+} yield, the Xe^+ yield shows a sharp rise at a time delay of zero, followed by a slower decrease as a function of the time delay. This behavior indicates that the NIR pulse probes another much faster process, which is the transient population of highly excited states of neutral atomic fragments that can be ionized by the NIR pulse. The highly excited states are populated during the XFEL pulse of 10 fs. Such a short time indicates that the excitations are created during nanoplasma formation and not afterwards

when they can be produced by, for example, the three-body recombination of quasi-free plasma electrons. The most probable mechanism is the inelastic scattering of the Auger electrons emitted during the initial cascade from neutral atoms in a cluster. The population of neutral excited states is expected to be depleted by a variant of interatomic Coulombic decay (ICD) in which two excited atoms exchange energy, ionizing one of them and deexciting the other. As many highly excited xenon atoms are created in the cluster, a cascade of such ICD processes is expected. The present experiments allow us to gain a fundamental insight into the ultrafast reactions induced by XFEL pulses, which should also be of crucial relevance for the use of XFEL pulses to determine the structure of nanosize objects “before destroy.” The present femtosecond time-resolved method is versatile and can be widely applied to study electron and nuclear dynamics induced by the interaction of hard XFEL pulses with any form of matter.

Chemical dynamics in the atomic clusters

When clusters are irradiated by an XFEL pulse with relatively low fluence, a series of oligomer formations, i.e., chemical dynamics triggered by X-rays, are observed.

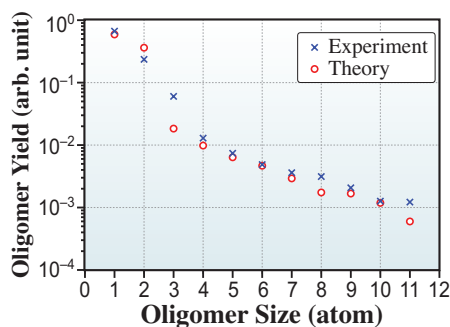


Fig. 6. Ar fragment yield as a function of the oligomer size at the photon energy of 5.5 keV and a peak fluence of $4.1 \mu\text{J}/\mu\text{m}^2$. [6]

Figure 6 depicts the yield of fragments from an Ar cluster ($\langle N \rangle \sim 1000$) as a function of the oligomer size at a photon energy of 5.5 keV and a peak fluence of $4.1 \mu\text{J}/\mu\text{m}^2$ [6]. Using a dedicated molecular dynamics simulation tool, we found that van der Waals bonding, the oligomer formation mechanism, and charge transfer among the cluster constituents significantly affect ionization dynamics induced by an XFEL pulse. The oligomer formation is due to bond formation between neutral atoms and an atomic ion, both during the early stage of cluster ionization when the first ions appear, and during cluster fragmentation when cluster components begin to move apart. Our results clearly demonstrate that XFEL pulses can be used not only to damage and destroy molecular assemblies but also to modify and transform their molecular structure.

Hironobu Fukuzawa^{a,b}, Kiyoshi Ueda^{a,b,*}

^aInstitute of Multidisciplinary Research for Advanced Materials, Tohoku University
^bRIKEN SPring-8 Center

*Email: kiyoshi.ueda@tohoku.ac.jp

References

- [1] T. Ishikawa *et al.*: Nat. Photonics **6** (2012) 540.
- [2] H. Fukuzawa *et al.*: Phys. Rev. Lett. **110** (2013) 173005.
- [3] K. Motomura *et al.*: J. Phys. Chem. Lett. **6** (2015) 2944.
- [4] K. Nagaya *et al.*: Phys. Rev. X **6** (2016) 021035.
- [5] T. Tachibana *et al.*: Sci. Rep. **15** (2015) 10977.
- [6] Y. Kumagai *et al.*: Phys. Rev. Lett. **120** (2018) 223201.
- [7] Y. Kumagai *et al.*: Phys. Rev. X **8** (2018) 031034.
- [8] M. Yabashi *et al.*: Appl. Sci. **7** (2017) 604.
- [9] H. Fukuzawa *et al.*: Nucl. Instrum. Meth. Phys. Res. A **907** (2018) 116.
- [10] T. Katayama *et al.*: Struct. Dyn. **3** (2016) 034301.